AGE AND ORIGIN OF ALBIAN GLAUCONITES AND ASSOCIATED CLAY MINERALS INFERRED FROM A DETAILED GEOCHEMICAL ANALYSIS

DAVY ROUSSET,[1]* SYLVIE LECLERC,[2] NORBERT CLAUER,[1] JOËL LANCELOT,[2] MICHEL CATHELINEAU,[3] AND JEAN-FRANÇOIS ARANYOSSY[4]

[1] *Centre de Géochimie de la Surface (CNRS/ULP), 1 rue Blessig, 67084 Strasbourg, France*
[2] *GdR FORPRO (CNRS-ANDRA), Espace GIS, Parc Scientifique Georges Besse, 150 rue Georges Besse, 30035 Nîmes, France*
[3] *UMR CNRS G2R et CREGU, B.P. 239, 54506 Vandoeuvre-lès-Nancy Cedex, France*
[4] *ANDRA, Parc de la Croix Blanche, 1/7 rue Jean Monnet, 92298 Châtenay-Malabry Cedex, France*
email: davyr@earth.ox.ac.uk

ABSTRACT: **Glauconitic grains are abundant in sandstones and siltstones from Albian and Cenomanian (transition between Lower and Upper Cretaceous) formations of southeastern France. Morphological and crystal-chemical data show that the ''green grains'' can be considered as glauconite *s.s.*, with minute amounts of pyrite, dolomite, calcite, and other clay minerals as grain coatings or crack fillings. Glauconite grains formed early during sedimentation, generally from detrital chlorite, biotite, or clay particles, and were found scattered together with other detrital mineral phases (muscovite, quartz) in the silt, in which porosity was considerably reduced afterwards by four stages of carbonate (calcite, dolomite) cementation.**

Geochemical data, especially the Fe, U, and Ce contents of the glauconitic grains, strongly suggest increasing oxidizing conditions with time in the sedimentation environment. The detailed geochemical analyses also allow the pristine glauconite grains to be distinguished from the other clay minerals occurring in the sequence. This enabled K–Ar and Rb–Sr dating of the glauconitic material, which yields identical results of 97.9 ± 0.4 and 97.9 ± 3.5 Ma, respectively. These dates point to a synsedimentary origin for the glauconites during the Late Albian (about 97–98 Ma). The K–Ar data also indicate that the Albian–Cenomanian boundary should be placed at 96.0 ± 1.9 Ma. The similarity between the K–Ar and Rb–Sr ages precludes any further significant pervasive recrystallization of these minerals during burial of the sequence either by heat flux or fluid flow. The K–Ar study of the clay matrix from the same siltstones suggests synsedimentary precipitation of additional clay minerals, probably together with the glauconite grains, such as mixed-layer illite–smectite identified in the clay size fraction of the sedimentary succession.

INTRODUCTION

Glauconitic minerals have been described in various continental or oceanic environments, mostly at shallow water depths (outer shelf and slope), where sedimentation rates are low (Amorosi 1997). They can be first approximated to dioctahedral mica, with higher K and Fe contents than illite (McRae 1972). Odin and Matter (1981) restricted the term glauconite to a dark-green, mica-type mineral often occurring in a granular shape with K_2O contents higher than 6 wt.%. The term glaucony was then proposed to refer to all other morphological glauconitic species corresponding to a continuous mixing between an Fe-rich smectite and a glauconitic mica as end members. Glauconites are actually considered to form by a two-step process: neoformation of an Fe-rich precursor (smectite) in various porous substrates, followed by K_2O incorporation leading to formation of a glauconitic mica during recrystallization of the precursor with concomitant dissolution of the substrate. This process, which seems to succeed best when induced by a worm digestion process, has been shown, by isotopic studies (Sr, Nd, and oxygen), to occur in recent to present-day glauconies (Clauer et al. 1992a; Clauer et al. 1992b; Stille and Clauer 1994).

Glaucony formation takes place during sediment deposition, at the water–sediment interface, thus providing materials suitable for dating the time of sediment deposition by isotopic methods (Odin 1982; Amireh et al. 1998). To ensure that the dated glauconites lack a detrital component and thus can provide meaningful stratigraphic ages, Odin (1975) suggested that only glauconites with K_2O contents higher than 6.5 wt.% should be used for isotopic dating. However, recent K–Ar dating of low-K_2O content glauconites, which have been buried at shallow depths, also yielded reliable ages (Téllez Duarte and López Martinez 2002).

The Cretaceous formations (Upper Albian and Cenomanian) of the southeastern French basin are glauconite-enriched siltstones and sandstones. Vertical sampling within these formations have recently been made possible by drilling carried out by the French National Agency for Radioactive Waste Management (ANDRA), to evaluate their physical and chemical characteristics for the construction of an underground test laboratory for disposal of radioactive waste. Albian siltstones and sandstones of the area consist of sand- or clay-rich layers ranging from one millimeter to several centimeters thick that are highly bioturbated and cemented by carbonate. After bioturbation in the sand-rich layers, the porosity of the silt has been reduced considerably during four stages of carbonate cementation (Cathelineau et al. 2001): (1, 2) two episodes of calcite formation (I & II) generated coatings and epigenetic calcite on bioclasts, and large euhedral calcite crystals that encased detrital grains (especially quartz) during growth; (3) zoned dolomite crystals formed after calcite II, commonly with ankerite overgrowths; and (4) the last episode of cement formation consisted mainly of xenomorphic calcite (III) crystallization, reducing the residual porosity. Mixed-layer illite–smectite was also observed in vugs (bioclasts) and is thought to form after calcite I and before calcite III precipitation. Previous studies (Orberger and Pagel 2000; Cathelineau et al. 2001) have shown that early glauconite grains represent the first authigenic mineral phase, forming during early diagenesis from several habits (pellets, bioclasts, feldspar infillings, and replacement of detrital minerals such as chlorite or micas) resulting in varied shapes for the glauconite grains.

The aim of this study is, on the basis of geochemical and isotopic results from glauconite and from the clay size fractions from the surrounding siltstones and the nearby sandstones, to decipher a possible relationship between the clay matrix and the diagenetic glauconite. Furthermore, these results provide useful information about the sedimentary conditions of the Albian sequence, as well as a reliable geochronological reference of the Albian–Cenomanian boundary, by K–Ar and Rb–Sr glauconite dating. Such information is needed for the understanding of the specific characteristics of this sedimentary sequence (low permeability and porosity induced during early diagenesis), and for the setting of a geochronological reference, which will be useful to estimate an epoch of fluid flow through faults in the sequence.

GEOLOGICAL SETTING

The sedimentary sequence, mostly Mesozoic in age, is about 8000 m thick. It lies on a Paleozoic crystalline basement located in southeastern

* Present address: Department of Earth Sciences, University of Oxford, Parks Road, Oxford OX1 3PR, U.K.

JOURNAL OF SEDIMENTARY RESEARCH, VOL. 74, NO. 5, SEPTEMBER, 2004, P. 631–642
 1527-1404/04/074-631/$03.00

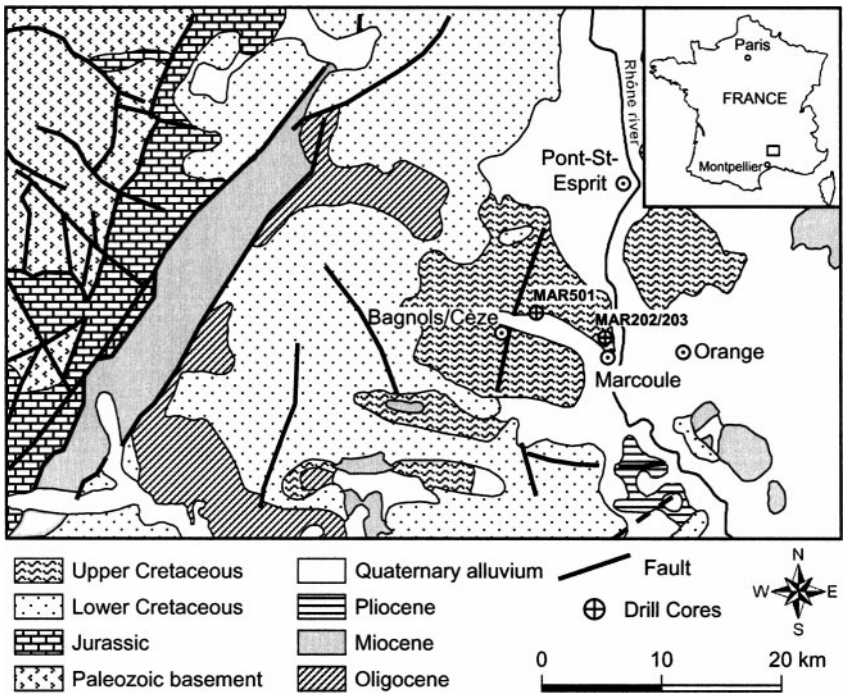

FIG. 1.—Location map of the studied area and location of the drill cores.

France between the Massif Central and the Alps, and formed part of the Tethys paleomargin (Fig. 1). Our study focused on the Cretaceous (Upper Albian–Lower Cenomanian), corresponding to clayey-silty sediments which overlie Lower Aptian (Urgonian) limestones (Masse 2000). The study site is located near Bagnols-sur-Cèze (Fig. 1), where the sedimentary succession consists of terminal Albian marls sandwiched between uppermost Albian and lowermost Cenomanian sandstones. The sequence geometry resulted from three successive geological events: (1) deposition about 100 Ma, (2) Pyrenean thrusting about 40 Ma, and (3) Messinian erosion about 5.4 Ma (ANDRA 1996). The thickness of the marly succession ranges from 157 to 404 meters according to borehole data (MAR501 and MAR202/203, respectively). Glauconite samples were collected from MAR202/203 boreholes, and the clay fractions of the matrix were extracted from samples of MAR501 borehole; the former are located at the ''Dent de Marcoule,'' which is a mountain overlooking the Messinian Cèze and Rhône paleovalleys, and the latter at the nearby edge of the Cèze paleovalley (Fig. 1).

SAMPLING AND METHODS

Glauconite grains were extracted from six samples collected at various depths in the Albian and Cenomanian siltstones and in the nearby Albian sandstones (Table 1, Fig. 2). They were first separated electromagnetically from clay material of the bulk rock, and then they were purified by hand picking with a needle under a binocular microscope (Leclerc 1999). Each initial fraction (called U) was washed with distilled water in an ultrasonic bath for 5 min (11 min for sample BAG 47) to separate the glauconite grains (called G) from adhering unconsolidated mud matter (called S). The pristine grains (G) were then separated from suspended mud (S) by centrifugation. The morphology, chemical composition, and homogeneity of the glauconite grains were determined by a qualitative and quantitative study using a JEOL JSM 840 scanning electron microscope (SEM) equipped with an X-ray microanalysis system (EDX TRACOR 5500). Analyses were done either spot by spot or along a traverse on a polished surface of grain.

TABLE 1.—*Glauconitic samples studied (MAR202/203 drill cores).*

Sample	Period	Depth (m)	Lithology
BAG 83	Cenomanian	435.0	Clayey siltstones and glauconitic sandstones
BAG 114	Albian	468.3	Clayey siltstones and glauconitic sandstones
BAG 28	Albian	468.5	Clayey siltstones and glauconitic sandstones
BAG 115	Albian	498.2	Clayey siltstones and glauconitic sandstones
BAG 47	Albian	790.2	Conglomeratic sandstones with glauconies
BAG 91	Albian	795.5	Conglomeratic sandstones with glauconies

The $< 2\ \mu$m clay fractions were extracted by sedimentation in distilled water from 21 whole-rock samples of MAR501 drill core, at various depths (Fig. 2). The rocks were first disaggregated by repetitive cycles of freeze–thaw to avoid contamination of the finest fractions by larger framework minerals reduced during crushing (Liewig et al. 1987). The $< 0.2\ \mu$m and 0.2–2 μm fractions were then separated from eight $< 2\ \mu$m fractions by using a high-speed centrifuge.

The contents of the major and trace elements of the clay minerals were determined by ICP-AES and ICP-MS, respectively, after tri-acid digestion of each sample in mixtures of HNO_3–HF–$HClO_4$. This method has the advantage of needing only a few milligrams of matter to complete all determinations, although it does not allow the determination of the amounts of Si, which evaporates by combination with F. The ICP analyses had overall analytical uncertainties of less than 10% (Samuel et al. 1985).

For K–Ar dating, the K amounts were determined from the same aliquots by atomic absorption, with a 2% precision controlled by regular determinations of international standards: the BEN basalt with an average of 1.39 $\pm$ 0.03 wt.% (2σ, $n = 6$) and the GLO glauconite with an average of 7.79 $\pm$ 0.15 wt.% (2σ, $n = 12$). For Ar determination, the samples were preheated under vacuum for at least 12 hours to remove the atmospheric Ar adsorbed to the particles, following a method close to that of Bonhomme et al. (1975). The analytical uncertainties were controlled by repetitive determination of the international GLO glauconite which averaged 24.59 $\pm$ 0.09 $\times$ 10^{-6}cm^3.g^{-1} (2σ, $n = 22$) radiogenic ^{40}Ar (^{40}Ar*), and of the ^{40}Ar/^{36}Ar ratio of the atmospheric Ar, which averaged 292.3 $\pm$ 2.5 (2σ, $n = 64$). The blanks of the mass spectrometer and the extraction line for the K–Ar dating were also determined, remaining systematically lower than 1×10^{-8}cm^3.g^{-1}.

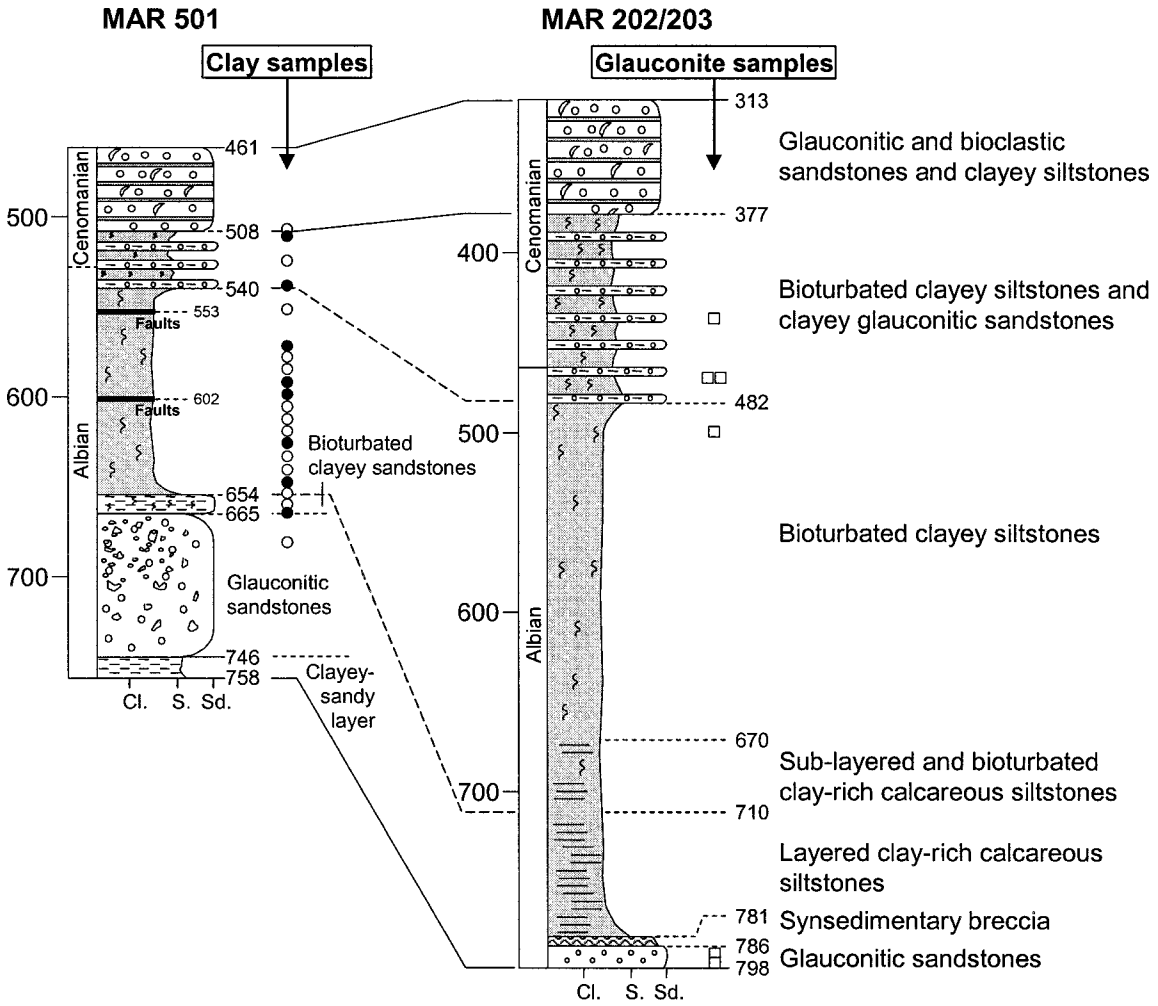

FIG. 2.—Stratigraphic log of MAR501 and MAR202/203 drill cores (modified from ANDRA 1996 and from Ferry 1999). Squares represent glauconite samples and circles clay fractions: open circles for < 2 μm fractions and filled circles for < 0.2, 0.2–2, and < 2 μm fractions.

The Sr isotopic compositions were determined by TIMS after Sr chromatographic separation on ion exchange resins following Birck's method (1979, 1986). The analytical precision of the TIMS equipped with five mobile collectors was periodically measured by determination of the $^{87}Sr/^{86}Sr$ ratio of the NBS987 standard which averages $0.710283 \pm 6 \times 10^{-6}$ (2σ, $n = 18$). The Rb/Sr ratios were obtained by ICP-MS. The Rb/Sr ratio of the international GLO glauconite averaged 13.16 ± 0.84 (2σ, $n = 10$) for a recommended value of 12.33 ± 0.58. In the following discussion, the Rb/Sr uncertainty is set at 10%. The standard decay constants were used for both methods (Steiger and Jäger 1977).

Isochron ages were calculated using linear weighted least-squares regression (Taylor 1997). The term ''weighted'' in this regard means that uncertainties in one measured parameter are known and used to weight each data point in the calculation of the straight-line parameters. Because in geochronology, both measured values are determined with uncertainties, the regression calculation is done in two steps, assuming, at each step, one dependent and one independent (no uncertainty) variables. The final result is the mean value of the two calculations, and the uncertainties include the largest variations obtained in each case.

RESULTS

Petrological Results

The sizes of the glauconite grains vary from 100 to 600 μm. The morphology ranges from typical rounded grains to various other shapes (Fig. 3 A–C). The grain surfaces are coated with disseminated crystals of calcite, pyrite, quartz and, more rarely, dolomite, or exhibit cracks filled with clayey or calcitic material. Some minerals intimately bound with surface defects could not be removed by ultrasonic treatment (Fig. 3D).

Analyses were performed on polished sections of several grains from BAG 28 and BAG 47 samples, allowing the calculation of structural formula of glauconitic grains, which shows no significant variations (Table 2). These results are confirmed by chemical analysis made along a cross section of a grain, which indicates a homogeneous chemical composition of the constitutive sheet silicates of the grains (Fig. 4). The analyses indicate that most grains are characterized by Si contents rather close to the reference values from Hendricks and Ross (1941) (Si between 3.7 and 3.8) and by an interlayer charge lower than reference glauconite (0.64 to 0.76). The Fe/Mg ratio is generally constant around 3 ± 0.5. The samples located above 550 m in MAR 202/203 boreholes are characterized by an increase in the Fe content (Fe/Mg ratio from 3.8 to 6.4; Cathelineau et al. 2001, this study), which we interpret as resulting from local redox conditions.

The < 2 μm clay fractions, which represent 10 to 30% of the whole rocks, consist mainly (55–80%) of mixed-layer illite–smectite (I–S) enriched in smectite layers ($S > 60\%$), together with small amounts of illite *s.l.* (micas, illite *s.s.*, glauconite), kaolinite, and traces of chlorite. Glauconite was found mainly in the nearby sandstones, and its occurrence is also suspected in samples collected next to the boundaries of the siltstone sequence. The XRD patterns of corresponding powdered preparations out-

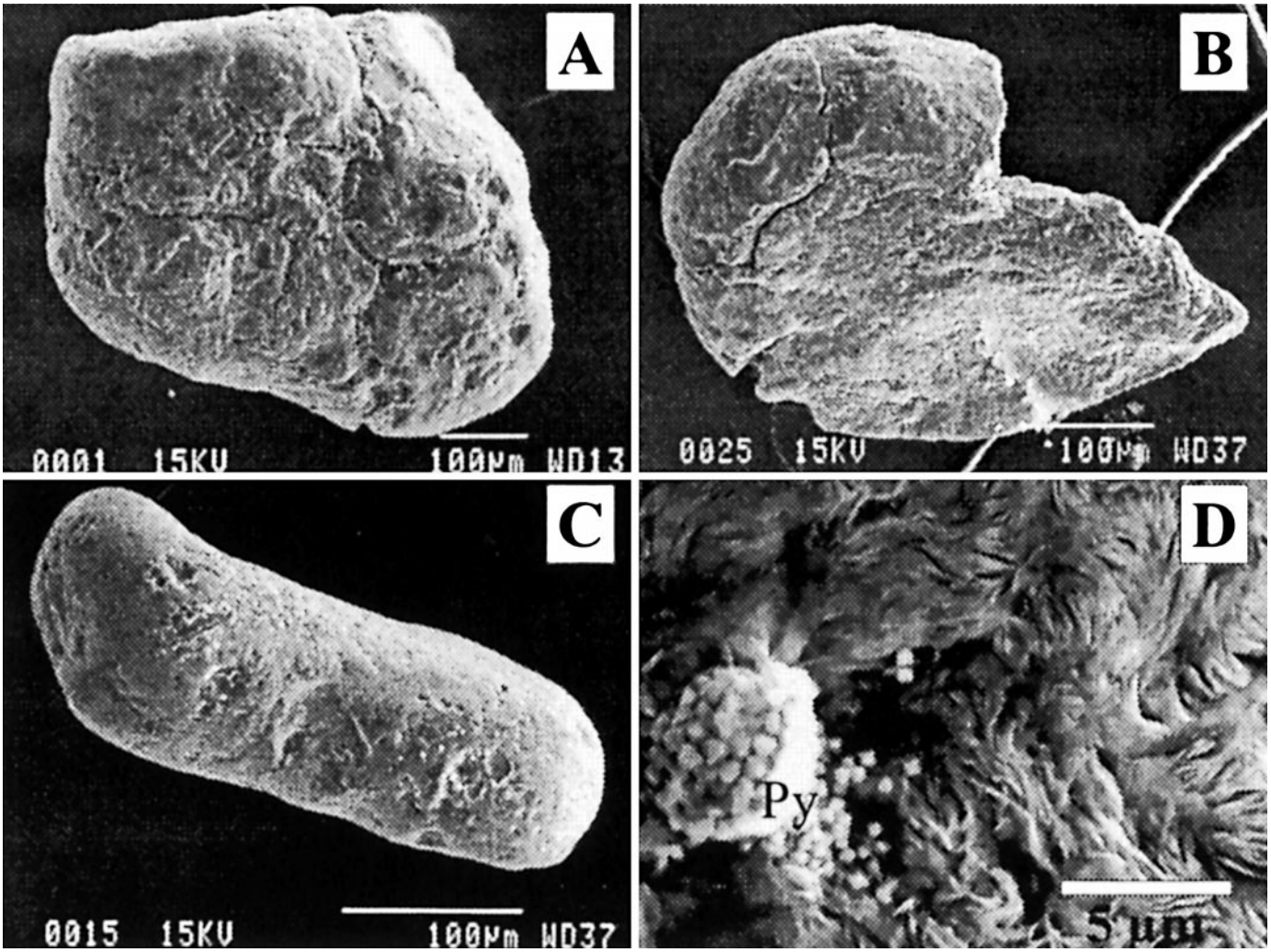

FIG. 3.—SEM photographs. **A–C)** Various grain morphologies. **D)** An ultrasonically treated glauconite grain surface. This treatment did not remove all the accessory minerals from the glauconite sheets, e.g., pyrite (Py).

TABLE 2.—*Calculated structural formula (expressed for half of a unit cell) from SEM semiquantitative analyses of polished surfaces of glauconite grains (Boldface, analyses performed on the grain edge; regular type, analyses performed on the inner part of the grains).*

Sample	Si	$Al_{tetra.}$	$Al_{octa.}$	Fe^{III}	Mg	Ca	K	Charge Deficit		Interlayer Charge
								Tetrahedral	Octahedral	
BAG 47 grain a	**3.70**	**0.30**	**0.30**	**1.26**	**0.44**	**0.02**	**0.72**	**0.30**	**0.45**	**0.75**
	3.81	**0.19**	**0.37**	**1.17**	**0.45**	**0.00**	**0.68**	**0.19**	**0.50**	**0.68**
	3.68	**0.32**	**0.25**	**1.28**	**0.47**	**0.00**	**0.78**	**0.32**	**0.46**	**0.78**
	3.67	**0.33**	**0.30**	**1.29**	**0.43**	**0.00**	**0.72**	**0.33**	**0.38**	**0.72**
	3.77	0.23	0.41	1.15	0.44	0.00	0.69	0.23	0.46	0.69
	3.70	0.30	0.29	1.23	0.48	0.00	0.76	0.30	0.46	0.76
	3.75	0.25	0.33	1.21	0.43	0.01	0.74	0.25	0.51	0.77
	3.82	0.18	0.34	1.23	0.36	0.02	0.69	0.18	0.55	0.73
BAG 47 grain b	**3.73**	**0.27**	**0.43**	**1.11**	**0.45**	**0.03**	**0.70**	**0.27**	**0.49**	**0.75**
	3.77	**0.23**	**0.53**	**1.02**	**0.44**	**0.01**	**0.69**	**0.23**	**0.48**	**0.71**
	3.76	**0.24**	**0.54**	**1.00**	**0.47**	**0.01**	**0.66**	**0.24**	**0.45**	**0.69**
	3.73	0.27	0.51	1.05	0.46	0.02	0.62	0.27	0.39	0.66
	3.77	0.23	0.49	1.05	0.45	0.00	0.72	0.23	0.49	0.72
	3.82	0.18	0.46	1.08	0.41	0.02	0.70	0.18	0.56	0.75
BAG 28	**3.73**	**0.27**	**0.22**	**1.44**	**0.31**	**0.01**	**0.63**	**0.27**	**0.37**	**0.65**
	3.88	**0.12**	**0.84**	**0.88**	**0.23**	**0.00**	**0.49**	**0.12**	**0.37**	**0.49**
	3.74	**0.26**	**0.22**	**1.47**	**0.26**	**0.01**	**0.67**	**0.26**	**0.42**	**0.68**
	3.75	0.25	0.22	1.42	0.33	0.02	0.63	0.25	0.42	0.67
	3.63	0.37	0.13	1.60	0.25	0.02	0.68	0.37	0.34	0.71
	3.71	0.29	0.26	1.45	0.24	0.00	0.67	0.29	0.38	0.67

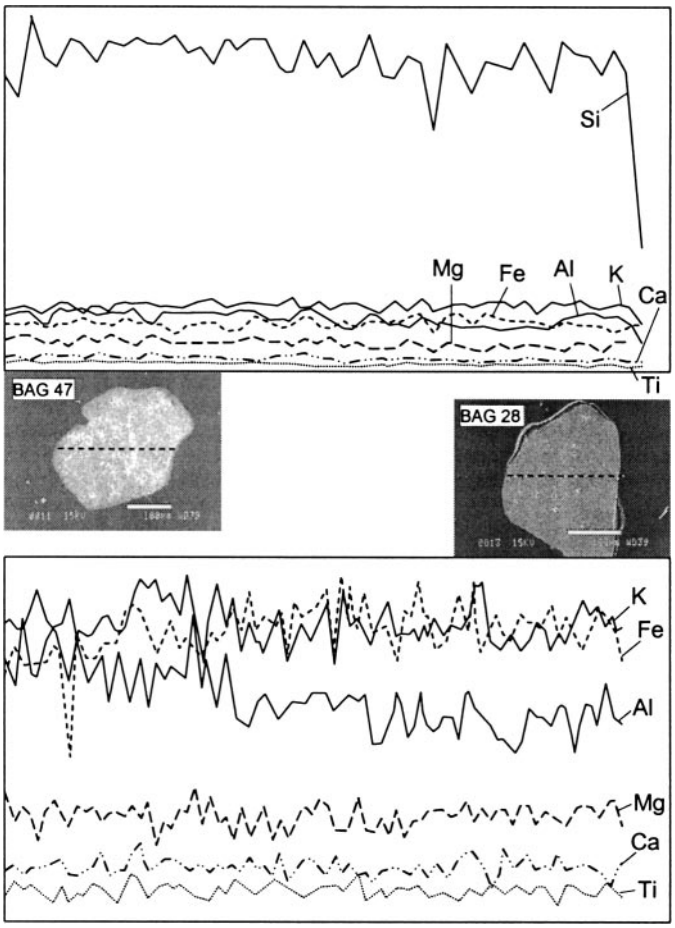

FIG. 4.—Chemical composition profiles of polished surfaces of two glauconite grains. Profiles are given by the dotted lines in the photographs (scale bar: 100 μm).

lined two broad peaks around 1.5 Å, which could be interpreted as the *b* parameter (*d*060 peak) of coexisting glauconite and illite (Moore and Reynolds 1989).

Geochemistry

The chemical compositions in Appendix 1 (see Acknowledgments) for glauconite grains (G) and suspended matter (S), derived from ultrasonic treatment of the grains, exhibit slight but significant variations between the two fractions. The K_2O content ranges from 5.90 to 6.99 wt.% in the grains, and it ranges from 4.39 to 7.16 wt.% in the mud removed from grains. Lower Fe_2O_3 and higher Al_2O_3 contents were obtained in the S fractions relative to the G separates (Appendix 1). These variations induce a slight displacement of the data points representative of the S fraction to the left in the Al_2O_3–MgO–Fe_2O_3 ternary diagram (Fig. 5) towards the field of the clay matrix (see below), without modifying the position of the data points in the CaO–Na_2O–K_2O diagram. The largest variations are observed for the BAG 28 sample, which is characterized by a significant increase in the Al_2O_3 content and a decrease of the K_2O content in the S fraction relative to the G fraction. Similarly, the Fe/Mg and Ca/Mg elementary ratios remain more or less constant between G and S, except for sample BAG 28 (Appendix 1). The Fe_2O_3 content and interlayer charge of all studied glauconite separates are characteristic of a glauconite-type mica, as defined by Odin and Matter (1981).

The S fractions are mostly enriched in trace elements (e.g., Ba, Zr, Rb, Pb, Th, U, and Sr to a lesser extent). The K/Rb ratio is systematically higher in the G fractions because of a combined decrease of Rb and an increase of K: $(K/Rb)_S$ = 162–209 and $(K/Rb)_G$ = 233–279 (Appendix 1). The U/Th ratio increases in the S fraction, implying the lower mobility of Th compared to U, except for sample BAG 28, for which the ratio remains about the same. The S fractions are also REE-enriched despite very low contents in both the G and S fractions ($< 100\ \mu g.g^{-1}$, Appendix 1). The REE patterns of the glauconitic material show systematic depletions in HREE, which is common for glauconites (Bonnot-Courtois 1981). The REE patterns yield also a systematic positive Ce anomaly, especially in the G fractions (Fig. 6).

The clay fractions from the siltstones contain essentially Al in octahedral position, whereas those from the surrounding sandstones and from the boundaries of the siltstones are enriched in Fe (Appendix 2, see Acknowledgments), which define two distinct areas for these lithologies in the ternary diagrams (Fig. 5).

The ultrasonic treatment does not seem to modify the geochemical characteristics of the glauconite grains significantly. The K/Rb ratio and the Al_2O_3 contents of the S suspended loads tend towards values of the clay minerals from nearby Albian siltstones, suggesting removal of these clays from cracks of the glauconitic grains. Indeed, the slight variations of the Fe_2O_3, MgO, and CaO contents between G and S fractions do not suggest preferential removal of pyrite, calcite, or dolomite from grains into the mud fractions, except for the Ca contents of sample BAG 28, which might be due to a contribution of calcite, in addition to that of clay particles suggested by the Fe, Al, and Mg contents in the S fractions.

In summary, SEM observations and chemical analyses show that most of the morphological and chemical characteristics of both the G and the S fractions result from dominant occurrence of glauconite micas, and that the minerals filling the grain cracks do not contribute strongly to the compositional analyses. However, the chemical differences in the major and trace elements between the G and S fractions show that some other minerals are preferentially concentrated in the suspended mud extracted from glauconite grains by ultrasonic treatment; it means that the detailed study of the glauconite grain fractions after ultrasonic treatment appears most likely to yield worthwhile results although accessory minerals can still occur in grain cracks.

The determination (''*r*'') matrix (Table 3) of the grain chemistry shows strong negative relationships among Fe and both Al and Mg, outlining the occurrence of Al–Fe octahedral substitutions in the glauconites, as already shown in many previous studies (Buckley et al. 1978; Ireland et al. 1983; Velde 1985; Dasgupta et al. 1990; Jarrar et al. 2000). However, the lack of correlation between Fe and K disproves here a criterion of glauconitic mineral evolution as suggested by Valeton et al. (1982), Jarrar et al. (2000), or Lee et al. (2002) among others. Similarly, no relationship between Fe and K was observed by Odin and Matter (1981) or Amorosi (1997).

Table 3 also shows positive correlations among Y, U, Th, ΣREE, and P, suggesting the occurrence of a phosphate-type mineral. The lack of correlation with Zr content excludes the presence of zircon.

K–Ar Results

Because the S and G fractions do not outline significant chemical variations, the K–Ar dating method was applied to both fractions and the dates were compared to those obtained on the corresponding untreated glauconites (U). All the K–Ar dates range from 88.9 ± 3.1 to 110.2 ± 4.3 Ma, from 92.6 ± 2.8 to 102.1 ± 2.5 Ma, and from 88.7 ± 2.6 to 103.1 ± 3.0 Ma for the S, G, and U fractions, respectively (Table 4).

If the $^{40}Ar/^{36}Ar$ and $^{40}K/^{36}Ar$ data were plotted on an isochron diagram, the points would fit a line with a *y* intercept of 198.5 ± 4.4 and a slope giving a date of about 106.1 ± 2.1 Ma using linear least-squares regression. The age decreases to 97.3 ± 0.4 Ma when the *y* intercept is forced through the atmospheric ratio, at 292.3 ± 2.5 as shown in Fig. 7A. This age value agrees with that found by Leclerc (1999) of 95.8 ± 5.9 Ma for five un-

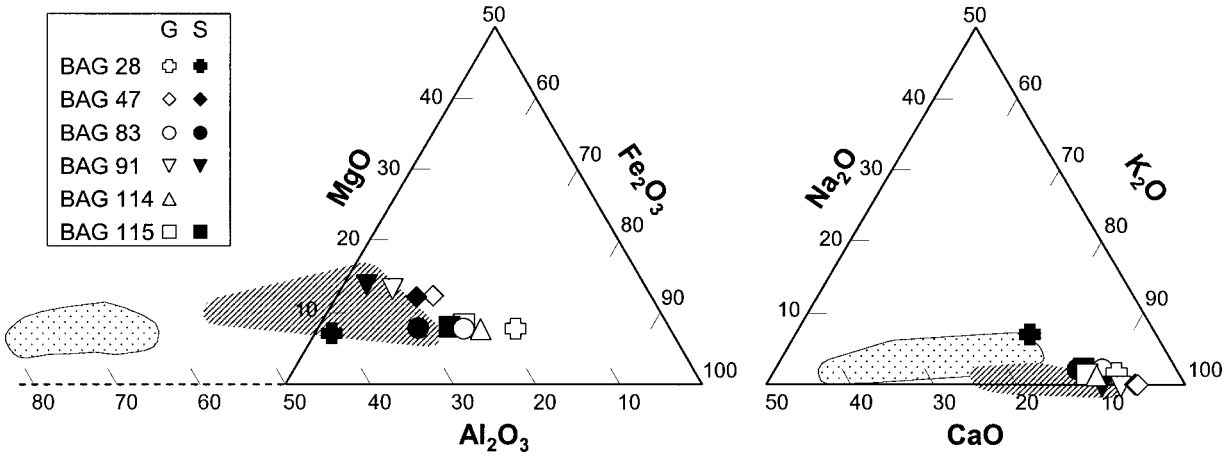

FIG. 5.—Chemistry of G (open symbols) and S (filled symbols) fractions plotted in the Al_2O_3–MgO–Fe_2O_3 and CaO–Na_2O–K_2O ternary diagrams. Hatched area corresponds to the clay fractions from the nearby sandstones and from the boundaries of Albian siltstones. The dotted area stands for the Albian clay fractions from siltstones.

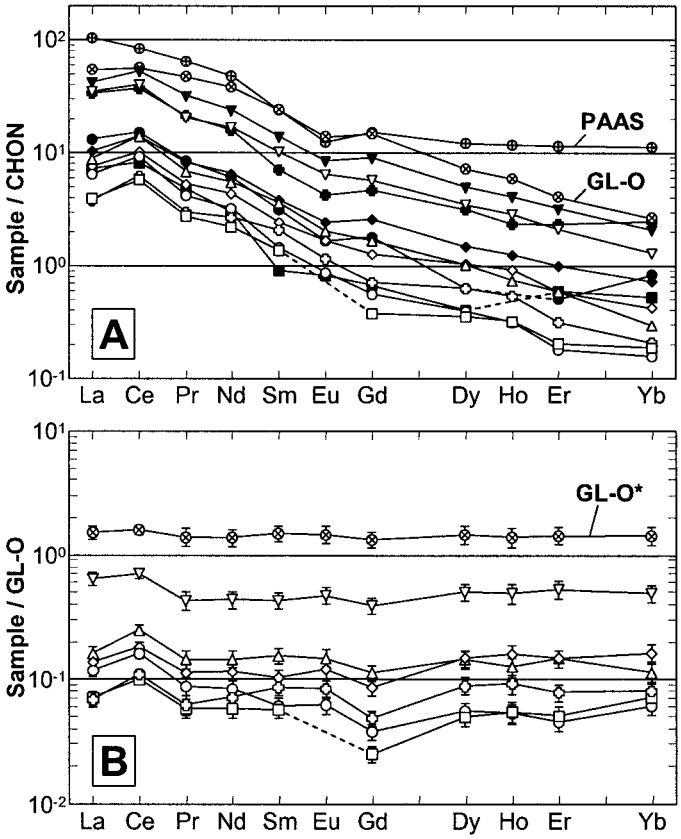

FIG. 6.—**A)** CHON-normalized REE patterns of G and S fractions (symbol legends in Fig. 5). Patterns of the PAAS and GL-O international standards are also reported. HREE depletion is a common characteristic in glauconites. Values of standards are from McLennan (1989) and Govindaraju (1995). **B)** GL-O-normalized REE patterns of G fractions. GL-O* stands for mean GL-O values analyzed as internal standard during this study ($n = 12$). It shows REE contents 1.5 times higher than expected values but demonstrates especially that the Ce positive anomaly is not an analytical artifact in the glauconites investigated. Error bars corresponds to relative error of analyzed GL-O standards. Dotted line means below detection limits.

treated Albian glauconies (BAG 06, 114, 28, 115, and 47). Isochron diagrams are rarely used for K–Ar dating purposes because the initial ratio is generally assumed to be the atmospheric ratio, so that each determination can provide a date directly, although the initial $^{40}Ar/^{36}Ar$ ratio can be different in specific cases (e.g., in Clauer and Chaudhuri 1995). Forcing the K–Ar isochron to go through the atmospheric $^{40}Ar/^{36}Ar$ ratio is done here to better constrain a mean age of glauconite formation, given that these minerals formed in the same sedimentary conditions during a short time interval.

The K–Ar dates of the clay fractions range from 98.9 ± 4.3 Ma to 176.3 ± 9.5 Ma, from 104.0 ± 3.3 to 236.2 ± 9.7 Ma, and from 140.6 ± 4.2 to 233.8 ± 7.0 Ma for the < 0.2 μm, < 2 μm, and 0.2–2 μm fractions of the same samples, respectively (Table 5). The lowest K–Ar values are found in each size fraction of the samples belonging to the nearby sandstones or to the lowermost Albian siltstones (654–665 m depth). The < 0.2 μm fraction of the sample at 664 m depth yields a K–Ar date of 98.9 ± 4.3 Ma, which is close to the theoretical age of the Upper Albian unit and to that obtained for the glauconite separates. The XRD pattern of a powdered preparation (see Petrological Results) of this sample suggests the occurrence of glauconite-type minerals in the clay fractions of this sample, which might explain the low K–Ar date. With the exception of the glauconite particles, the K–Ar dates of the clay fractions from siltstones are systematically greater than the stratigraphic age, but the youngest dates for any sample are to be found in the finest fractions (Table 5). This feature has already been found in similar sedimentary sequences and discussed at length (Clauer and Chaudhuri 1995; Rousset and Clauer 2003) as reflecting mixtures of at least two clay populations: a detrital (old) and an authigenic (young) one.

Plotted in an isochron diagram, $^{40}Ar/^{36}Ar$ vs. $^{40}K/^{36}Ar$, the data points of the clay material not of glauconitic origin fit a line that yields a geologically meaningless value of 217 ± 14 Ma and a *y* intercept of 271 ± 7, close to the atmospheric ratio (Fig. 8). The line in the diagram might be considered as resulting from a mixture, following Faure's (1986) definition. In general, the detrital (older) particles are found in the coarsest fractions (0.2–2 μm) and the authigenic (younger) particles in the finest fractions (< 0.2 μm). The samples containing glauconite, such as those from the boundaries of the sedimentary sequence and the nearby sandstones, plot away from the previous mixing line and fit along a line nearly parallel to the theoretical 100 Ma line (Fig. 8). Glauconite appears to represent a third end member to the previous binary mixture, with high K_2O and low radiogenic ^{40}Ar contents.

TABLE 3.—*Determination matrix for the chemical data of the studied glauconitic micas (Grain fractions).*

	Al	Mg	Ca	Fe	Mn	Ti	Na	K	P	Sr	Ba	V	Cr	Sc	Y	Zr	Co	Rb	Pb	Th	U
Al	1																				
Mg	**0.74**	1																			
Ca		−0.54	1																		
Fe	**−0.91**	**−0.93**		1																	
Mn	0.6	**0.7**	−0.66	**−0.75**	1																
Ti	**0.72**			−0.65	**0.76**	1															
Na	−0.69	**−0.96**		**0.87**	−0.65	−0.46	1														
K		0.56					**−0.73**	1													
P	**0.83**	**0.86**		**−0.86**			**−0.86**	0.48	1												
Sr	**−0.78**	**−0.77**		**0.85**	**−0.94**	**−0.85**	**0.78**		−0.57	1											
Ba	−0.66	**−0.99**	0.63	**0.87**	−0.69		**0.95**	−0.61	**−0.81**	**0.74**	1										
V	0.63	**0.93**	−0.67	**−0.85**	**0.87**	0.55	**−0.92**	0.6	0.66	**−0.89**	**−0.94**	1									
Cr	**0.71**	**0.95**	−0.59	**−0.92**	**0.85**	0.59	**−0.94**	0.53	**0.73**	**−0.89**	**−0.94**	**0.98**	1								
Sc					**0.75**	0.69	−0.57	0.57		**−0.81**	−0.47	**0.71**	0.62	1							
Y	**0.79**	**0.7**		−0.69	0.48	0.48	**−0.7**	0.48	**0.76**	−0.69	−0.67	0.63	0.61	0.55	1						
Zr						0.69								**0.72**		1					
Co	0.59	0.63	**−0.7**	−0.63	**0.83**	0.5	−0.48			**−0.77**	−0.64	**0.71**	0.66	0.58	0.65		1				
Rb		**0.87**	**−0.83**	−0.67	0.59		**−0.75**	0.48	0.6	−0.53	**−0.92**	**0.82**	**0.79**		0.49		0.67	1			
Pb	−0.67	**−0.88**		**0.84**	−0.49		**0.94**	−0.63	**−0.88**	0.64	**0.85**	**−0.79**	**−0.85**		−0.53			−0.61	1		
Th	0.69								0.57						**0.83**					1	
U	**0.76**	**0.9**		**−0.83**	0.46		**−0.81**		**0.9**	−0.59	**−0.89**	**0.73**	**0.75**		**0.81**		0.61	**0.82**	**−0.73**	0.54	1
Ce^*_{pn}	**−0.83**	**−0.96**		**0.94**	−0.6		**0.86**		**−0.91**	0.68	**0.92**	**−0.8**	**−0.86**		−0.68		0.6	**−0.82**	**0.83**		**−0.94**
Eu^*_{pn}								−0.58							**−0.82**					**−0.7**	−0.55
La/Yb_{pn}	0.68								0.6						**0.89**		0.47			**0.98**	0.65
ΣREE	**0.78**	**0.75**		**−0.72**			−0.68		**0.91**		**−0.72**	0.52	0.56		**0.87**		0.47	0.6	−0.62	**0.76**	**0.94**

The determination coefficient *r* is a statistical value traducing the occurrence or the lack of correlation between two parameters. *r* tending towards 1 or 0 means strong or no relationship respectively. Furthermore, the sign of *r* indicates a positive or negative correlation. Only significant correlation values are given: regular type ≡ $|r| > 0.45$; bold type ≡ $|r| > 0.70$.

Eu_{pn} and Ce_{pn} stand for Eu and Ce anomalies, and $(La/Yb)_{pn}$ for the coefficient of fractionation, all calculated form PAAS-normalized REE contents.

Rb–Sr Dating

The Rb–Sr dating method was applied only to the G fractions, to avoid detrital occurrence. The variation among the Rb/Sr and the $^{87}Sr/^{86}Sr$ ratios is large enough to use an isochron diagram $^{87}Sr/^{86}Sr$ vs. $^{87}Rb/^{86}Sr$ (Table 4, Fig. 7B). The calculation provides an age of 97.9 ± 3.5 Ma, which agrees with the K–Ar date calculated previously. In addition, the initial $^{87}Sr/^{86}Sr$ ratio of 0.70736 ± 0.00014 corresponds well to the Sr-isotope composition of the Cretaceous seawater of 0.7073 ± 0.0001 (Hess et al. 1986; McArthur et al. 1993; Jones et al. 1994; Lancelot et al. 1998; Lancelot 1999; Leclerc 1999) and to the $^{87}Sr/^{86}Sr$ ratio of three Aptian belemnites sampled in the studied area (0.70731 ± 0.00003; Lancelot 1999; Leclerc 1999). This leads to conclude that the Rb–Sr dates can be considered as dating the crystallization of the glauconite micas in a marine environment.

DISCUSSION

Relationship among Glauconites and Clay Fractions

Many of the results obtained (e.g., XRD, geochemistry, K–Ar) suggest the occurrence of Fe-rich glauconite at the boundaries of the Albian siltstones and in the associated sandstones. This is seen in the plot of K_2O vs. $(Fe_2O_3 + MgO)$ (Fig. 9). The clay fractions from Albian siltstones have K_2O and $Fe_2O_3 + MgO$ concentrations below 2.1 and 8 wt.%, respectively, whereas those from the sandstones and from the boundaries of the siltstones tend towards higher values, indicating the occurrence of a glauconite mineral phase in the clay fractions. These latter fractions, enriched in glauconite particles, yield chemical compositions close to those of the G glauconite fractions (Fig. 5), whereas the clay fractions from Albian siltstones are enriched in Al and depleted in K relative to the former. As mentioned above, the slight variations among the G and S fractions could be consid-

TABLE 4.—*K–Ar and Rb–Sr analyses of glauconies.*

Sample	Depth (m)	F[a]	K_2O (wt. %)	$^{40}Ar_{rad}$ (10^{-6} $cm^3 \cdot g^{-1}$ STP)	$^{40}Ar_{rad}$ (%)	$^{40}Ar/^{36}Ar$	$^{40}K/^{36}Ar$ ($\times 10^3$)	K–Ar Age (Ma ± 2σ)	Rb ($\mu g \cdot g^{-1}$)	Sr ($\mu g \cdot g^{-1}$)	$^{87}Rb/^{86}Sr$	$^{87}Sr/^{86}Sr$ (± 2σ × 10^{-6})
BAG 83	435.0	U[b]	6.24	19.86	66.27	876 ± 4	101.1 ± 0.7	96.1 (3.0)				
		S	5.49	16.13	58.38	710 ± 6	78.2 ± 0.5	88.9 (3.1)				
		G	6.10	19.03	68.02	924 ± 4	111.3 ± 0.5	94.3 (2.9)	202.88	121.36	4.82	0.713675 (16)
BAG 06	466.5	U[b]	6.68	19.58	70.80	1012 ± 10	135.5 ± 1.9	88.7 (2.6)				
BAG 114	468.3	U[b]	6.19	21.17	70.44	1000 ± 7	114.1 ± 1.0	103.1 (3.0)				
		G	6.72	21.14	73.24	1104 ± 10	141.9 ± 1.4	95.0 (2.7)	190.00	139.36	3.93	0.713116 (14)
BAG 28	468.5	U[b]	6.98	20.68	63.87	818 ± 3	97.7 ± 0.5	89.6 (2.9)				
		S	4.96	18.18	52.79	626 ± 11	50.0 ± 1.5	110.2 (4.3)				
		G	6.96	21.33	68.39	935 ± 3	115.3 ± 0.4	92.6 (2.8)	219.31	207.02	3.05	0.711359 (16)
BAG 115	498.2	U[b]	6.40	21.30	67.59	912 ± 3	102.6 ± 0.5	100.4 (3.1)				
		S	6.01	18.10	68.77	946 ± 20	119.7 ± 5.3	91.1 (2.7)				
		G	6.50	20.32	72.58	1078 ± 2	138.1 ± 0.3	94.4 (2.7)	191.09	158.96	3.46	0.712399 (13)
BAG 47	790.2	U[b]	7.89	24.74	78.64	1383 ± 14	192.3 ± 2.6	94.7 (2.5)				
		S	7.52	23.31	74.86	1175 ± 23	157.3 ± 4.0	93.7 (2.6)				
		G	7.39	25.03	84.76	1939 ± 5	267.1 ± 0.6	102.1 (2.5)	235.87	54.89	12.39	0.724525 (15)
BAG 91	795.5	S	7.14	21.79	67.95	922 ± 7	113.8 ± 0.6	92.2 (2.8)				
		G	7.43	24.14	85.28	2008 ± 16	290.0 ± 2.7	98.0 (2.4)	241.67	89.25	7.80	0.718182 (13)

[a] Fraction: U = Untreated glauconites (initial grains) − G = Grains after ultrasonic treatment − S = Suspended matter after ultrasonic treatment.
[b] Data from Leclerc (1999).

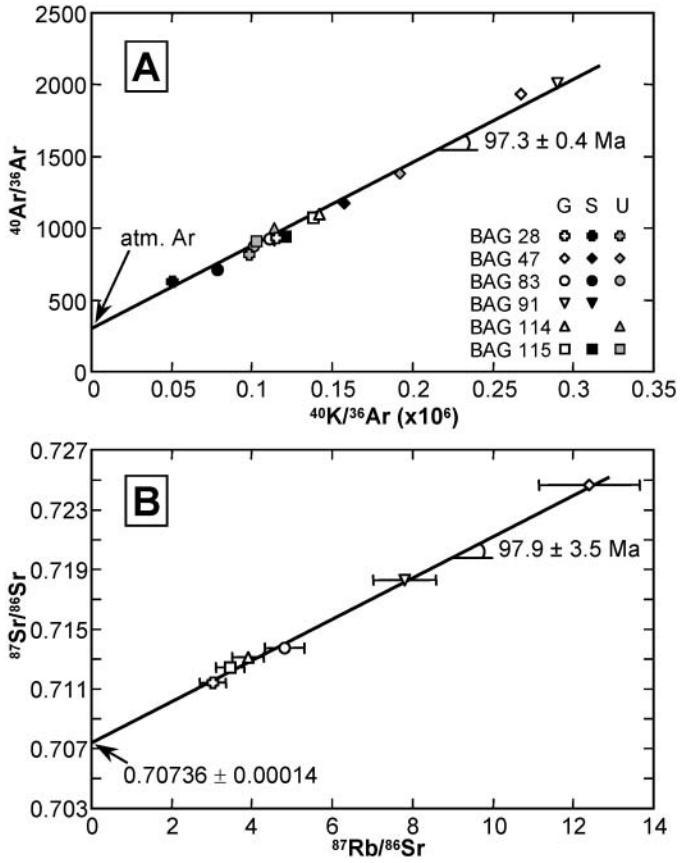

FIG. 7.—**A)** K–Ar dates for glauconitic fractions (S = suspended matter and G = grain after ultrasonic treatment of the untreated fractions U) plotted in an isochron diagram. **B)** G samples plotted in a Rb–Sr isochron diagram.

ered as reflecting the contribution of clay particles in the S fractions, removed from cracks of the glauconite grains.

The overall K–Ar dates of the clay fractions suggest that at least three end members could be mixed in the materials analyzed: detrital particles resulting from the weathering of the continental crystalline basement, glauconite grains crystallizing during deposition of the sediments, and a younger clay mineral. The latter could correspond to the identified mixed-layer illite–smectite that precipitated during an early diagenetic stage, soon after deposition.

The Process of Glauconitization in the Albian Sediments

Systematic depletion of HREE in glauconite grains is common (Bonnot-Courtois 1981), pointing to a formational process related to the occurrence of organic matter, which is known to preferentially scavenge HREE (Hoyle et al. 1984). The REE patterns of the G glauconite separates also yield a systematic positive Ce anomaly (Fig. 6). This Ce anomaly basically relates to oxidizing conditions, which induce a change of the Ce oxidation state from +III to +IV and a decrease of the ionic radius of ca. 15%. The tetravalent Ce can then be incorporated in oxides as well as Fe or Mn (e.g., by Mn oxides, inducing a negative anomaly in the seawater). This positive Ce anomaly is in contradiction to the depletion in HREE found in the same REE patterns. It supports a two-step evolution, as for recent glauconite (Clauer et al. 1992a; Clauer et al. 1992b; Stille and Clauer 1994): an initial crystallization of smectite under redox conditions different from those occurring during K incorporation into the glauconitic layers. Alternately, the Ce anomaly may also result from other processes during diagenesis (Murray et al. 1991) such as LREE fractionation, which seems not to be the case here. On the other hand, Shimizu and Masuda (1977) and Fleet et al. (1980) interpreted a positive Ce anomaly in cherts and subaerial glauconites as resulting from a specific behavior of Ce in marginal or shelf seas during the Cretaceous (no depletion in Ce), which might be the case here.

Many attempts have been made to link Ce anomalies to paleo-redox conditions (e.g., Courtois and Clauer 1980; Liu et al. 1988; Wilde et al. 1996). We considered this process to explain the relationship between Ce anomaly and Fe_2O_3 contents, inasmuch as Odin and Matter (1981) and Amorosi (1997) concluded that the fixation of Fe precedes the incorporation of K during glauconitization. Therefore, the correlation obtained here between Ce anomaly and Fe content means that the Ce anomaly relates to the formation of the Fe-rich smectite precursor (Table 3). Recently, Kelly and Webb (1999) have shown that glauconitization in Oligo-Miocene sandstones occurred under suboxic, partially reducing conditions. The suboxic conditions are assumed to favor mobilization and incorporation of trivalent Fe, which is the main Fe species in glauconite (e.g., Jarrar et al. 2000; Giresse and Wiewióra 2001). The occurrence of a positive Ce anomaly might then be considered as reflecting oxidizing conditions during the Fe-smectite precipitation stage.

The positive Ce anomaly is greater for high Fe_2O_3 contents but also correlates with low U content (Fig. 10); these variations also change with depth and lithology (see Table 1 for corresponding data). Uranium is known to be sensitive to the redox changes in the sediments, because in more reduced conditions highly soluble hexavalent U, which occurs as $UO_2(CO_3)_2^{2-}$ complex in sea water (Cochran 1992), becomes insoluble tetravalent U, easily precipitated as UO_2 oxides. Although at low concentration U could be also adsorbed onto clay minerals or organic matter, the U contents in sediments are then expected to be higher in more reducing conditions (Henderson and Anderson 2003). Thus, the trend observed in Figure 10 might reflect stronger oxic conditions from the lower ($\approx$ 790 m depth) to the upper sandstones and siltstones ($\approx$ 470 m), resulting in higher Fe and lower U contents in glauconite. On the basis of data from organic matter in the same boreholes, Fleck et al. (2002) assume that changes in redox conditions could be due to bioturbation in relation to the more oxic conditions in the sediments. As a local anoxic event prevented bioturbation at the base of the Albian siltstones in the MAR203 borehole (Ferry 1999), this assumption supports the change in the redox conditions observed here.

The depletion in HREE found in the REE patterns of glauconite, in apparent contradiction to the positive Ce anomaly, might then represent either the chemical fingerprint of the substrate or the result of K incorporation into the mineral interlayer, which should then have occurred in a reducing environment brought about by the presence of organic matter. The strong correlation between HREE fractionation (La/Yb ratio) and both Y and Th contents could represent the chemical signature of monazite, a phosphate which is enriched in LREE, Y, and Th and depleted in HREE (McLennan 1989). Nonetheless, there are arguments against a monazite influence in this case: (1) the lack of correlation between (La/Yb) and P contents (Table 3), (2) absence of a negative Eu anomaly in glauconite grains which is characteristic of monazite as well as HREE depletion, and (3) petrologic studies revealed no trace of monazite in the siltstones (Orberger and Pagel 2000; this study).

Timing of Glauconitization

The closeness of the K–Ar dates obtained from the glauconite grains and from the clay material removed after ultrasonic treatment demonstrates that the suspended clay consists mostly of particles having an age close to that of pristine glauconite. Alternatively, the old K–Ar date of the S fraction of sample BAG 28 (110.2 $\pm$ 4.3 Ma) points to the occurrence of older clay materials, probably originating from clay minerals of the surrounding siltstones, for which the K–Ar data outline an overall contribution of a detrital component.

Furthermore, the K–Ar dating of the separated and treated glauconite

TABLE 5.—*K–Ar analyses of the clay fractions from Albian siltstones and surrounding sandstones.*

Fraction	Sample[a]	Depth (m)	K_2O (wt. %)	$^{40}Ar_{rad}$ (10^{-6} $cm^3 \cdot g^{-1}$ STP)	$^{40}Ar_{rad}$ (%)	$^{40}Ar/^{36}Ar$	$^{40}K/^{36}Ar$ ($\times 10^3$)	Age (Ma $\pm$ 2σ)
<2 μm	MAR 17297	507	4.21	14.53	65.82	864.60	91	**104.0** (3.3)
	MAR 17306	510	2.48	18.28	53.72	638.55	26	**215.4** (8.7)
	MAR 17341	524	1.87	12.03	53.96	641.88	30	**189.3** (7.5)
	MAR 17376	538	2.20	14.48	46.45	551.85	22	**193.4** (8.8)
	MAR 17430	551	1.93	15.70	52.04	616.13	22	**236.2** (9.7)
	MAR 17494	571	1.98	14.10	15.32	348.94	4	**208.5** (30.3)
	MAR 18818	577	2.10	12.87	68.73	945.07	59	**180.8** (5.8)
	MAR 18858	584	1.81	13.90	56.26	675.56	27	**223.8** (8.6)
	MAR 18870	591	1.83	14.83	56.24	675.28	26	**235.4** (9.0)
	MAR 18891	598	1.67	11.31	59.04	721.48	35	**198.9** (7.3)
	MAR 17502	605	1.84	14.23	57.95	702.81	16	**225.3** (8.4)
	MAR 17521	612	1.81	12.19	60.15	741.49	37	**197.7** (7.1)
	MAR 17543	618	1.91	12.82	64.53	833.06	44	**197.1** (6.7)
	MAR 18970	625	1.93	14.55	60.27	743.68	33	**220.0** (7.9)
	MAR 18986	632	2.14	13.86	56.52	679.62	33	**190.6** (7.2)
	MAR 17576	640	2.44	15.31	39.62	489.42	17	**184.9** (9.7)
	MAR 17581	647	2.20	13.34	48.24	570.90	25	**178.9** (7.8)
	MAR 17602	653	2.91	19.23	54.12	644.02	29	**194.2** (7.6)
	MAR 17588	659	4.26	22.75	48.15	569.94	28	**158.5** (6.8)
	MAR 17622	664	5.85	25.58	50.30	595.00	38	**130.7** (5.3)
	MAR 17622d			24.94	43.02	518.56	29	**127.6** (6.1)
	MAR 18926	680	4.73	19.25	54.57	650.48	48	**122.1** (4.6)
	MAR 18926d		4.58	18.31	55.56	664.90	51	**120.0** (4.5)
<0.2 μm	MAR 17306	510	2.40	11.56	29.66	420.07	14	**143.6** (9.9)
	MAR 17376	538	2.51	12.67	27.79	409.23	12	**150.2** (11.1)
	MAR 17494	571	2.13	10.58	30.04	422.38	14	**147.9** (10.0)
	MAR 18870	591	2.39	14.27	38.96	484.07	18	**176.3** (9.5)
	MAR 18891	598	1.93	9.66	32.04	434.80	15	**149.0** (9.6)
	MAR 18970	625	2.38	11.88	39.69	489.97	22	**148.6** (7.7)
	MAR 17581	647	2.81	13.37	30.52	425.29	15	**141.9** (9.6)
	MAR 17622	664	7.00	22.93	47.00	557.55	44	**98.9** (4.3)
0.2–2 μm	MAR 17306	510	2.32	14.87	66.95	893.98	52	**188.7** (6.2)
	MAR 17376	538	2.06	14.60	60.91	756.00	36	**207.6** (7.4)
	MAR 17494	571	1.80	13.66	66.30	876.91	42	**221.3** (7.4)
	MAR 18870	591	1.69	13.60	76.66	1265.81	67	**233.8** (7.0)
	MAR 18891	598	1.68	11.17	66.87	892.00	50	**195.4** (6.5)
	MAR 18970	625	1.76	12.57	76.00	1231.44	73	**209.0** (6.3)
	MAR 17581	647	1.90	13.05	62.30	783.92	39	**201.4** (7.1)
	MAR 17622	664	5.92	27.89	68.93	951.03	77	**140.6** (4.2)

[a] d = Duplicates.

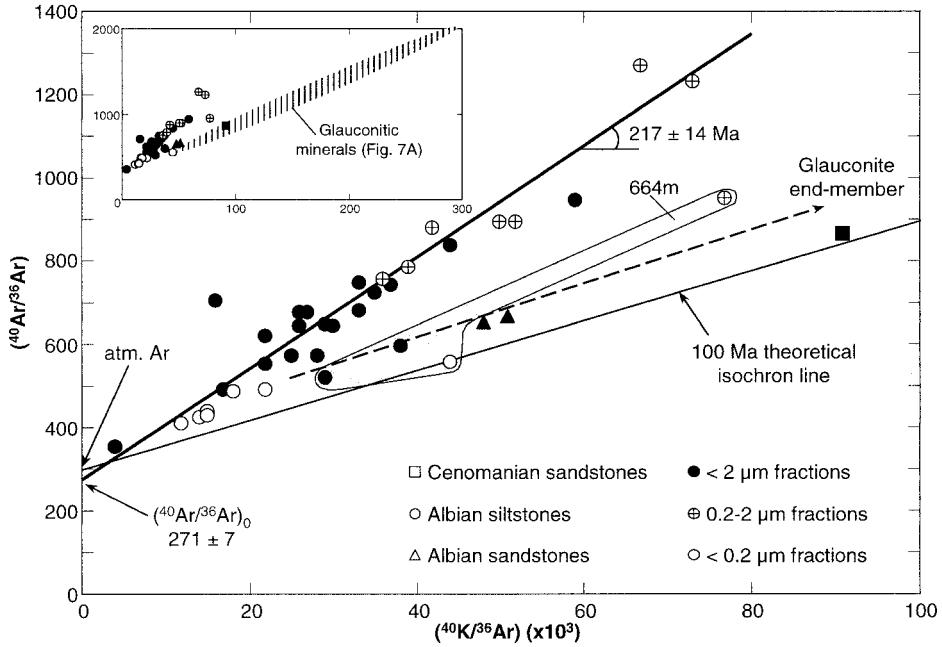

FIG. 8.—K–Ar dates for clay fractions plotted in an isochron diagram. Grey area corresponds to the 664 m depth clay fractions. The left-hand insert compares the clay data points with the glauconitic minerals (Fig. 7A).

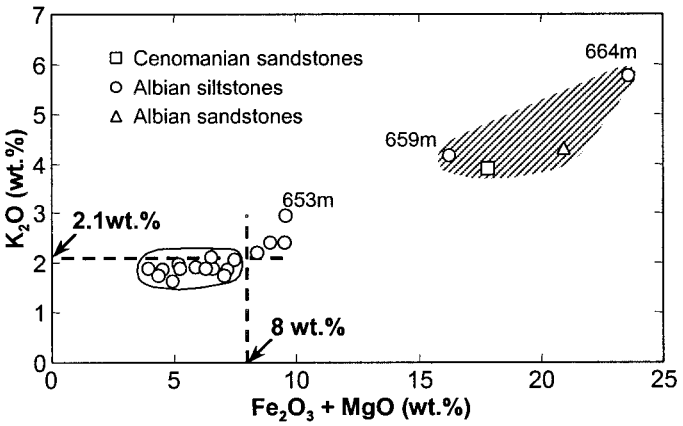

FIG. 9.—Relationships between the K_2O contents and the (Fe_2O_3 + MgO) contents in the clay matrix (< 2 μm fractions). Hatched area corresponds to the clay fractions from the nearby sandstones and from the boundaries of Albian siltstones.

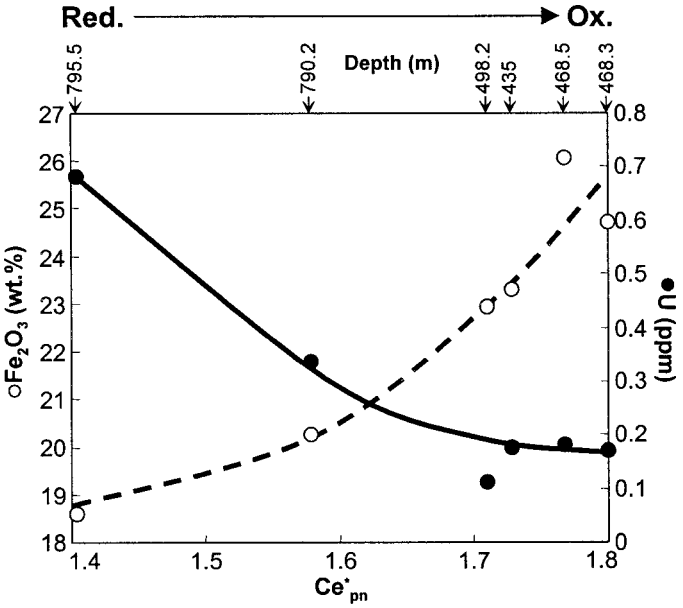

FIG. 10.—Fe_2O_3, U, and Ce behaviors in glauconite grains. The diagram reflects change of redox conditions, from reducing conditions (Red.) in the left-hand side to more oxidant ones (Ox.) in the right-hand side. The redox conditions seem to vary with depth.

grains provided an age of 97.9 ± 0.4 Ma, which is identical to that obtained by Rb–Sr dating on the same aliquots, at 97.9 ± 3.5 Ma. The debate about the reliability of K–Ar and Rb–Sr dating methods applied to glauconites is not recent (e.g., Montag and Seidemann 1981, 1982a, 1982b; Keppens and Pasteels 1982; Odin and Gale 1982; Harris et al. 1984). Although this paper is not dedicated to such a study, the similar ages obtained from two different and independent methods strongly support the fact that the ages are reliable and that the mean age of the sedimentary sequence can be placed at 97–98 Ma. Because the K–Ar system of clays and glauconies is much more sensitive to later modifications than the Rb–Sr system (Clauer 1981), the identical ages from two chemically different isotopic systems indicate that no further pervasive recrystallization effect affected the glauconite grains, either by heat flux or fluid flow after deposition of the sediments; otherwise the K–Ar ages would have to be younger than the Rb–Sr ages (Clauer et al. 2003).

Estimation of the Age of the Albian–Cenomanian Boundary

The glauconites from the upper sandy layers (≈ 430–500 m depth in the MAR202/203 drill core) frame the Albian–Cenomanian boundary (Fig. 2). This boundary was well defined by ammonite distribution in the MAR203 borehole (Amédro and Robaszynski 1997) at a depth of ca. 460 m. On the basis of the K–Ar dates obtained from glauconite minerals in the same depth interval (435–498.2 m), an age of 96.0 ± 1.9 Ma can be proposed for the Albian–Cenomanian boundary in the region. This age is in agreement with previous estimates of this boundary elsewhere, i.e., 96 Ma (Odin and Odin 1990) and 97 Ma (Harland et al. 1990) but slightly lower than the most recent proposal of 98.9 ± 0.6 Ma (2σ) by Gradstein et al. (1995). In fact, this latter value is older because the authors did not compile the low-temperature dates, such as those obtained from glauconite dating, assuming that such minerals (i.e., those with closure temperature < 250 °C, Harland et al. 1990) yield younger ages than high-temperature minerals (e.g., Gradstein et al. 1988).

It is true that for periods older than 115 Ma, low-temperature dates are systematically lower than high-temperature ones and should be regarded as minimum ages (Harland et al. 1990), but the Albian–Cenomanian boundary is clearly a younger event. Interestingly enough, Gradstein et al. (1995) reported ages for the Albian–Cenomanian boundary for low-temperature dates that are 2.3 Ma lower, at a mean value of 96.62 ± 0.46 Ma (1σ), which is within the range of ages found here. In conclusion, the age for the Albian–Cenomanian boundary calculated here from K–Ar dating of glauconite grains, is in the range of published values if using both low- and high-temperature dating methods.

Reliability of Glauconite Dating

Reliable K–Ar and Rb–Sr dates can be derived from glauconite only with a careful sample selection and purification by geochemical and mineralogical checking, as already suggested by Odin (1975). Ultrasonic treatment removed most of the accessory minerals intimately bound with glauconite grains, especially K-rich clay minerals from surrounding rocks, which could have biased K–Ar results. Variations of the major-element and trace-element concentrations between the grain and the suspended matter extracted after ultrasonic treatment demonstrates the preferential removal of these clays minerals (Fig. 5 and Appendix 1, see Acknowledgments).

Furthermore, the sedimentary sequence studied here was buried at shallow depths. The burial temperature remained probably lower than 50–70°C according to the fluid-inclusion data in quartz and the total immaturity of the organic matter (Cathelineau et al. 2001). This low burial temperature probably favors Ar retention in silicate sheets, leading to reliable and concordant K–Ar and Rb–Sr ages.

CONCLUSIONS

A study of glauconite grains and clay particles from Cretaceous sedimentary basin of southeastern France shows that glauconite crystallized during deposition of the clayey-silty-sandy sediments. This synsedimentary origin constrains the Late Albian in this area to about 97–98 Ma and enables us to estimate the age of the Albian–Cenomanian boundary at 96.0 ± 1.9 Ma. The K–Ar and Rb–Sr dates of glauconite separates were found to be very similar, providing ages of 97.9 ± 0.4 Ma and 97.9 ± 3.5 Ma, respectively. These identical ages negate the possibility of pervasive recrystallization of clay minerals after glauconite formation, either by heat flux or fluid flow, which would have caused the Rb–Sr and K–Ar ages to be different. The closeness of these dates can also be explained by the low burial temperature of the sedimentary sequence as well as by the careful mineralogical and geochemical analysis of the glauconite grains, which allowed us to date pure glauconite minerals. Further, the geochemical results strongly suggest that redox conditions probably became more oxidizing during sediment deposition, as recorded by Fe, U, and Ce variations in

glauconite grains according to depth (this study) and supported by previous results on organic matter (Cathelineau et al. 2001; Fleck et al. 2002).

In addition, the K–Ar study of the clay matrix from Albian siltstones indicates that glauconite as well as other clay materials formed during early diagenesis, such as the authigenic mixed-layer illite–smectite identified in the sequence.

ACKNOWLEDGMENTS

The authors would like to acknowledge ANDRA for having made available the samples of drill cores and the technical staff of the CGS for assistance during the study. S. Hesselbo and S. Shaw are thanked for their comments on an early version of this manuscript. Constructive reviews and suggestions from P.D. Fullagar, H. Zwingmann, D. Awwiller, and D.A. Budd improved the manuscript significantly. This study was funded by the French National Center for Scientific Research (CNRS) and the French National Agency for Radioactive Waste Management (ANDRA) through the GdR FORPRO (ANDRA-CNRS Research Group) and corresponds to the GdR FORPRO contribution number FORPRO 2003/07 A. DR was funded through a State Department Research stipend. This is the EOST contribution number 2003.302-UMR7517.

The data in Appendix 1 and 2 have been archived and are available in digital form on the SEPM data archive, Address: SEPM Society for Sedimentary Geology, 6128 E. 38th Street, Suite #308, Tulsa, Oklahoma 74135-5814; email: kfarnsworth@sepm.org; URL: http://www.sepm.org/archive/index.html.

REFERENCES

Amédro, F., and Robaszynski, F., 1997, Datation précise en forage à l'aide des ammonites, *in* Etude du Gard Rhodanien, Atlas des posters des journées scientifiques CNRS/ANDRA (French National Center for Scientific Research/French National Agency for Radioactive Waste Management), Bagnols-sur-Cèze, October 20–21 1997: Paris, EDP sciences, p. GG1.

Amireh, B.S., Jarrar, G., Henjes-Kunst, F., and Schneider, W., 1998, K–Ar dating, X-Ray diffractometry, optical and scanning electron microscopy of glauconies from the early Cretaceous Kurnub Group of Jordan: Geological Journal, v. 33, p. 49–65.

Amorosi, A., 1997, Detecting compositional, spatial and temporal attributes of glaucony: a tool for provenance research: Sedimentary Geology, v. 109, p. 135–153.

ANDRA, 1996, Chapter II: renseignements d'ordre géologique et géophysique disponibles quant au caractère favorable des formations à étudier: Rapport ANDRA (French National Agency for Radioactive Waste Management), ANDRA/DIR/96/1138, 52 p.

Birck, J.L., 1979, Chronologie primitive des objets planétaires différenciés [Ph.D. thesis]: Paris, University of Paris VII, 280 p.

Birck, J.L., 1986, Precision K–Rb–Sr isotopic analysis: application to Rb–Sr chronology: Chemical Geology, v. 56, p. 73–83.

Bonhomme, M., Thuizat, R., Pinault, Y., Clauer, N., Wendling, R., and Winkler, R., 1975, Méthode de datation potassium–argon. Appareillage et technique: Institut de Géologie de Strasbourg, Note Technique, v. 3, 53 p.

Bonnot-Courtois, C., 1981, Géochimie des terres rares dans les principaux milieux de formation et de sédimentation des argiles [Ph.D. thesis]: Paris, University of Paris-Sud, 217 p.

Buckley, H.A., Bevan, J.C., Brown, K.M., and Johnson, L.R., 1978, Glauconite and celadonite: two separate mineral species: Mineralogical Magazine, v. 42, p. 373–382.

Cathelineau, M., Buschaert, S., Roubeuf, V., Mosser-Ruck, R., Boiron, M.C., Fleck, S., Elie, M., and Landais, P., 2001, Diagenèse des sédiments du site Est et du Gard: chronologie relative de la formation des minéraux argileux, paléothermicité et milieux de dépôt: Rapport final, Action 98/IV GdR FORPRO (French National Agency for Radioactive Waste Management (ANDRA) and French National Center for Scientific Research (CNRS) Research Group), 19 p.

Clauer, N., 1981, Rb–Sr and K–Ar dating of Precambrian clays and glauconies: Precambrian Research, v. 15, p. 331–352.

Clauer, N., and Chaudhuri, S., 1995, Clays in Crustal Environments; Isotope Tracing and Dating: Berlin, Springer-Verlag, 358 p.

Clauer, N., Keppens, E., and Stille, P., 1992a, Sr isotopic constraints on the process of glauconitization: Geology, v. 20, p. 133–136.

Clauer, N., Stille, P., Keppens, E., and O'Neil, J.R., 1992b, Le mécanisme de la glauconitisation: apports de la géochimie isotopique du strontium, du néodyme et de l'oxygène de glauconies récentes: Académie des Sciences (Paris), Comptes Rendus, Série II, v. 315, p. 321–327.

Clauer, N., Zwingmann, H., and Gorokhov, I.M., 2003, Postdepositional evolution of platform claystones based on a simulation of thermally induced diffusion of radiogenic ^{40}Ar from diagenetic illite: Journal of Sedimentary Research, v. 73, p. 58–63.

Cochran, J.K., 1992, The oceanic chemistry of the uranium and thorium series nuclides, *in* Ivanovich, M., and Harmon, R.S., eds., Uranium-Series Disequilibrium: Applications to Earth, Marine, and Environmental Sciences: Oxford, U.K., Oxford University Press, p. 334–395.

Courtois, C., and Clauer, N., 1980, Rare earth elements and strontium isotopes of polymetallic nodules from southeastern Pacific Ocean: Sedimentology, v. 27, p. 687–695.

Dasgupta, S., Chaudhuri, A.K., and Fukuoka, M., 1990, Compositional characteristic of glauconitic alterations of K-feldspar from India and their implications: Journal of Sedimentary Petrology, v. 60, p. 277–281.

Faure, G., 1986, Principles of Isotope Geology, Second Edition: New York, Wiley, 589 p.

Ferry, S., 1999, Apport des forages ANDRA de Marcoule à la connaissance de la marge crétacée rhodanienne, *in* Etude du Gard Rhodanien: Actes des journées scientifiques CNRS/ANDRA (French National Center for Scientific Research/French National Agency for Radioactive Waste Management), Bagnols-sur-Cèze, October 20–21 1997: Paris, EDP sciences, p. 63–91.

Fleck, S., Michels, R., Ferry, S., Malartre, F., Elion, P., and Landais, P., 2002, Organic geochemistry in a sequence stratigraphic framework. The siliciclastic shelf environment of Cretaceous series, SE France: Organic Geochemistry, v. 33, p. 1533–1557.

Fleet, A.J., Buckley, H.A., and Johnson, L.R., 1980, The rare earth element geochemistry of glauconites and celadonites: Geological Society of London, Journal, v. 137, p. 683–688.

Giresse, P., and Wiewióra, A., 2001, Stratigraphic condensed deposition and diagenetic evolution of green clay minerals in deep water sediments on the Ivory Coast–Ghana Ridge: Marine Geology, v. 179, p. 51–70.

Govindaraju, K., 1995, 1995 Working Values with Confidence Limits for Twenty-Six CRPG, ANRT and IWG-GIT Geostandards: Geostandards Newsletter, Special Issue, v. 19, p. 1–32.

Gradstein, F.M., Agterberg, F.P., Aubry, M.P., Berggren, W.A., Flynn, J.J., Hewitt, R., Kent, D.V., Klitgord, K.D., Miller, K.G., Obradovich, J.D., Ogg, J.G., Prothero, D.R., and Westermann, G.E.G., 1988, Sea level history: Science, v. 241, p. 599–601.

Gradstein, F.M., Agterberg, F.P., Ogg, J.G., Hardenbol, J., Van Veen, P., Thierry, J., and Huang, Z., 1995, A Triassic, Jurrassic and Cretaceous time scale, *in* Berggren, W.A., Kent, D.V., Aubry, M.P., and Hardenbol, J., eds., Geochronology, Time Scales and Global Stratigraphic Correlation: SEPM, Special Publication 54, p. 95–126.

Harland, W.B., Armstrong, R.L., Cox, A.V., Craig, L.E., Smith, A.G., and Smith, D.G., 1990, A Geological Time Scale 1989: Cambridge, U.K., Cambridge University Press, 265 p.

Harris, W.B., Fullagar, P.D., and Winters, J.A., 1984, Rb–Sr glauconite ages, Sabinian, Claibornian and Jacksonian units, southeastern Atlantic Coastal Plain, U.S.A.: Palaeogeography, Palaeoclimatology, Palaeoecology, v. 47, p. 53–76.

Henderson, G.M., and Anderson, R.F., 2003, The U-series toolbox for paleoceanography, *in* Bourdon, B., Henderson, G.M., Lundstrom, C.C., and Turner, S.P., eds., Uranium-Series Geochemistry: Reviews in Mineralogy and Geochemistry, v. 52, p. 493–531.

Hendricks, S.B., and Ross, C.S., 1941, Chemical composition and genesis of glauconite and celadonite: American Mineralogist, v. 26, p. 683–708.

Hess, J., Bender, M.L., and Schilling, J., 1986, Evolution of the ratio of strontium 87 to strontium 86 in seawater from Cretaceous to Present: Science, v. 231, p. 979–984.

Hoyle, J., Elderfield, H., Gledhill, A., and Greaves, M., 1984, The behaviour of the rare earth elements during mixing of river and sea waters: Geochimica et Cosmochimica Acta, v. 48, p. 143–149.

Ireland, B.J., Curtis, C.D., and Whiteman, J.A., 1983, Compositional variation within some glauconites and illites and implications for their stability and origins: Sedimentology, v. 30, p. 769–786.

Jarrar, G., Amireh, B., and Zachmann, D., 2000, The major, trace and rare earth element geochemistry of glauconites from the early Cretaceous Kurnub Group of Jordan: Geochemical Journal, v. 34, p. 207–222.

Jones, C.E., Jenkyns, H.C., Coe, A.L., and Hesselbo, S.P., 1994, Strontium isotopic variations in Jurassic and Cretaceous seawater: Geochimica et Cosmochimica Acta, v. 58, p. 3061–3074.

Kelly, J.C., and Webb, J.A., 1999, The genesis of glaucony in the Oligo-Miocene Torquay Group, southeastern Australia: petrographic and geochemical evidence: Sedimentary Geology, v. 125, p. 99–114.

Keppens, E., and Pasteels, P., 1982, Comment on the paper: ''A test of the reliability of Rb–Sr dates for selected glauconite morphologies of the Upper Cretaceous (Navesink Formation) of New Jersey,'' by R.L. Montag and D.E. Seidemann: Earth and Planetary Science Letters, v. 58, p. 439–441.

Lancelot, J., 1999, Discussion de l'évolution des isotopes radiogéniques dans la couche silteuse de Marcoule en domaines non fracturés et fracturés, *in* Etude du Gard Rhodanien, Actes des journées scientifiques CNRS/ANDRA (French National Center for Scientific Research/French National Agency for Radioactive Waste Management), Bagnols-sur-Cèze, October 20–21 1997: Paris, EDP sciences, p. 139–166.

Lancelot, J., Leclerc, S., Verdoux, P., and Aranyossy, J.F., 1998, A strontium and lead study of the Marcoule silty-clay series (Gard, France) and implications for characterisation of water–rock interactions in low permeability argillaceous media, *in* Fluid flow through Faults and Fractures in Argillaceous Formations: Proceedings of a joint Nuclear Energy Agency/European Commission Workshop, Berne, Switzerland, June 10–12 1996, p. 223–242.

Leclerc, S., 1999, Contribution de la méthode Rb/Sr à la démonstration de la qualité de confinement de la couche silteuse de Marcoule (Gard Rhodanien) [Ph.D. thesis]: Montpellier, University of Montpellier II, 208 p.

Lee, C.H., Choi, S.W., and Suh, M., 2002, High iron glaucony from the continental shelf of the Yellow Sea off the southwestern Korean Peninsula: Journal of Asian Earth Sciences, v. 20, p. 507–515.

Liewig, N., Clauer, N., and Sommer, F., 1987, Rb–Sr and K–Ar dating of clay diagenesis in Jurassic sandstone oil reservoir, North sea: American Association of Petroleum Geologists, Bulletin, v. 71, p. 1467–1474.

Liu, Y.G., Miah, M.R.U., and Schmitt, R.A., 1988, Cerium: A chemical tracer for paleooceanic redox conditions: Geochimica et Cosmochimica Acta, v. 52, p. 1361–1371.

Masse, J.P., 2000, Explanatory notes: Atlas peri-Tethys, Paris.

McArthur, M.A., Thirwall, M.F., Gale, A.S., Kennedy, W.J., Burnett, J.A., Mattey, D., and Lord, A.R., 1993, Strontium isotope stratigraphy for the Late Cretaceous: A new curve,

based on the English Chalk, *in* Hailwood, E.A., and Ridd, R.B., eds., High Resolution Stratigraphy: Geological Society of London, Special Publications 70, p. 195–209.

McLennan, S.M., 1989, Rare earth elements in sedimentary rocks: influence of provenance and sedimentary processes, *in* Lipin, B.R., and McKay, G.A., eds., Geochemistry and Mineralogy of Rare-Earth Elements: Reviews in Mineralogy, v. 21, p. 169–200.

McRae, S.G., 1972, Glauconite: Earth-Science Reviews, v. 8, p. 397–440.

Montag, R.L., and Seidemann, D.E., 1981, A test of the reliability of Rb–Sr dates for selected glauconite morphologies of the Upper Cretaceous (Navesink Formation) of New Jersey: Earth and Planetary Science Letters, v. 52, p. 285–290.

Montag, R.L., and Seidemann, D.E., 1982a, A test of the reliability of Rb–Sr dates for selected glauconite morphologies of the Upper Cretaceous (Navesink Formation) of New Jersey—Reply to the comment by E. Keppens and P. Pasteels: Earth and Planetary Science Letters, v. 58, p. 442.

Montag, R.L., and Seidemann, D.E., 1982b, A test of the reliability of Rb–Sr dates for selected glauconite morphologies of the Upper Cretaceous (Navesink Formation) of New Jersey—Reply to the comment by G.S. Odin and N.H. Gale: Earth and Planetary Science Letters, v. 58, p. 446–447.

Moore, D.M., and Reynolds, R.C., Jr., 1989, X-Ray Diffraction and the Identification and Analysis of Clay Minerals: Oxford, U.K., Oxford University Press, 332 p.

Murray, R.W., Buchholtzten Brink, M.R., Brumsack, H.J., Gerlach, D.C., and Price Russ, G., III, 1991, Rare earth elements in Japan Sea sediments and diagenetic behaviour of Ce/Ce*: Results from ODP Leg 127: Geochimica et Cosmochimica Acta, v. 55, p. 2453–2466.

Odin, G.S., 1975, De glauconarium constitutione, origine, aetateque [Ph.D. thesis]: Paris, University of Paris-Sud, 280 p.

Odin, G.S., 1982, How to measure glaucony ages, *in* Odin, G.S., ed., Numerical Dating in Stratigraphy: Chichester, U.K., John Wiley & Sons, p. 387–403.

Odin, G.S., and Gale, N.H., 1982, Some fundamental considerations in the dating of glauconies: a comment on ''A test of the reliability of Rb–Sr dates for selected glauconite morphologies of the Upper Cretaceous (Navesink Formation) of New Jersey,'' by R.L. Montag and D.E. Seidemann: Earth and Planetary Science Letters, v. 58, p. 443–445.

Odin, G.S., and Matter, A., 1981, De glauconarium origine: Sedimentology, v. 28, p. 611–641.

Odin, G.S., and Odin, C., 1990, Geologic time scale, calibrated in 1990: Geochronique, v. 35, p. 12–21.

Orberger, B., and Pagel, M., 2000, Diagenetic evolution of Cretaceous siltstones from drill core MAR501 (Southeastern France): Journal of Geochemical Exploration, v. 69–70, p. 115–118.

Rousset, D., and Clauer, N., 2003, Discrete clay diagenesis in a very low-permeable sequence constrained by an isotopic (K–Ar and Rb–Sr) study: Contributions to Mineralogy and Petrology, v. 145, p. 182–198.

Samuel, J., Rouault, R., and Besnus, Y., 1985, Analyse multiélémentaire standardisée des matériaux géologiques en spectrométrie d'émission par plasma à couplage inductif: Analusis, v. 13, p. 312–317.

Shimizu, H., and Masuda, A., 1977, Cerium chert as an indication of marine environment of its formation: Nature, v. 266, p. 346–348.

Steiger, R.H., and Jäger, E., 1977, Subcommission on geochronology: convention on the use of decay constants in geo- and cosmochronology: Earth and Planetary Science Letters, v. 36, p. 359–362.

Stille, P., and Clauer, N., 1994, The process of glauconitization: chemical and isotopic evidence: Contributions to Mineralogy and Petrology, v. 117, p. 253–262.

Taylor, J.R., 1997, An introduction to error analysis: the study of uncertainties in physical measurements, Second Edition: Sausalito, California, University Science Books, 327 p.

Téllez Duarte, M.A., and López Martinez, M., 2002, K–Ar dating and geological significance of clastic sediments of the Paleocene Sepultura Formation, Baja California, Mexico: Journal of South American Earth Sciences, v. 15, p. 725–730.

Valeton, I., Abdul-Razzak, A., and Klussmann, D., 1982, Mineralogy and geochemistry of glauconite pellets from Cretaceous sediments in northwest Germany: Geologisches Jahrbuch, v. 52, p. 5–93.

Velde, B., 1985, Clay Minerals: Amsterdam, Elsevier, Developments in Sedimentology, v. 40, 427 p.

Wilde, P., Quinby-Hunt, M.S., and Erdtmann, B.D., 1996, The whole-rock cerium anomaly: a potential indicator of eustatic sea-level changes in shales of the anoxic facies: Sedimentary Geology, v. 101, p. 43–53.

Received 10 January 2003; accepted 11 March 2004.